Journal of Molecular Liquids 337 (2021) 116612

Contents lists available at ScienceDirect

Journal of Molecular Liquids

journal homepage: www.elsevier.com/locate/molliq

Exploring the structural and catalytic features of lipase enzymes immobilized on g-C_3N_4: A novel platform for biocatalytic and photocatalytic reactions

Esra Bilgin Simsek [a,*], Didem Saloglu [b]

[a] Department of Chemical Engineering, Faculty of Engineering, Yalova University, 77100 Yalova, Turkey
[b] Disaster and Emergency Management Department, Disaster Management Institute, Istanbul Technical University, Maslak, 34730 Istanbul, Turkey

ARTICLE INFO

Article history:
Received 12 January 2021
Revised 16 March 2021
Accepted 27 May 2021
Available online 31 May 2021

Keywords:
Carbon nitride
Lipase
Immobilization
Biocatalyst
Photocatalysis

ABSTRACT

The exploration of multifunctional supporting materials for modern enzyme immobilization is an attractive subject for advanced catalytic applications. In the present study, lipase enzyme types, namely palatase 20,000 L, lipozyme TL100L, and lipozyme CALB, were immobilized on graphitic carbon nitride (g-C_3N_4) using physical and covalent immobilization methods in order to obtain biohybrids for utilization in biocatalytic and photocatalytic reactions. Characterization tests confirmed successful immobilization of enzymes without changing the crystal phase of g-C_3N_4. The immobilization yields were calculated as 71.0% and 93.4% for C_3N_4@PLTS; 81.3% and 95.4% for C_3N_4@LPZYM; and 79.4% and 91.7% for C_3N_4@CALB biohybrids using physical adsorption and covalent bonding methods, respectively. The kinetic constant values of K_m and V_{max} were significantly higher for immobilized lipases than for free forms. The photocatalytic efficiencies of biohybrid catalysts were also greater than raw g-C_3N_4. Among the lipase types, lipozyme TL100L attached on g-C_3N_4 exhibited the best catalytic performance in both biocatalytic and photocatalytic experiments, which was attributed to its open lid structure. As a result, this study opens the door to utilizing g-C_3N_4 as a support material for the immobilization of different enzymes and establishing catalyzed reactions.

1. Introduction

Enzymes have received growing attention and been utilized in extensive biotechnological and industrial sectors due to their high catalytic activities, high substrate specificity and moderate catalytic conditions in contrast to conventional catalysts [1]. Lipase enzymes (triacylglycerol ester hydrolase, E.C. 3.1.1.3) were well studied as catalysts because of their unique physicochemical features. Lipases are remarkably effective in versatile reactions, such as hydrolysis, esterification, transesterification, alcoholysis, and C–C bond formation [2]. They can catalyze chemical reactions in both hydrophobic and hydrophilic media and are also stable in organic or eutectic solvents and supercritical fluids which enables them to be applied in industrial biocatalysis [3]. Lipases have similar molecular structure consisting of a β-sheet and a catalytic triad of serine, histidine, and carboxylic acid. Their active sites can be quite different, which affects the substrate specificity and reaction mechanisms. All enzymes are adapted to operate at the interfaces of the solid–liquid phases [4]. This situation known as "interfacial activation" can be explained by combining the substrate characteristic and monomolecular film interface in an aqueous medium. In the absence of interfaces, lipases have some elements of secondary structures, called a "lid", covering their active sites and making them accessible/inaccessible to substrates [5]. Also, in hydrophobic interfaces, important conformational changes take place yielding the "open structure" of lipases [6]. These changes result in the exposure of hydrophobic parts, interacting with the hydrophobic interface, and conferring functionality to the enzyme.

However, free lipase enzymes suffer from low operational stability and they should be anchored on suitable networks to enhance the enzyme activity and recyclability as well as thermostability [7]. Therefore, chemical and physical immobilization methods were developed, namely adsorption, cross-linking, encapsulation and covalent binding [8,9]. Among them, immobilization via adsorption is considered the most useful method since it involves physical interactions including Van der Waals forces, electrostatic interactions, hydrogen bonding and ionic interactions [10]. Although the physical interactions are rather weak, the native structure as well as the activity of the enzyme can remain stable

* Corresponding author.
E-mail address: ebilgin.simsek@yalova.edu.tr (E. Bilgin Simsek).

https://doi.org/10.1016/j.molliq.2021.116612
0167-7322/

after immobilization [10,11]. Physical adsorption has also advantage like low-cost and chemical free binding properties [12]. Covalent bonding provides strong strength and overcomes the problem of leakage of enzymes caused by weak interactions in adsorption. The covalent attachment enables easy incorporation of crosslinkers with a variety of functional groups in the support material [11,13]. The lipase molecules with strong nucleophiles can interact with the electrophilic groups on the support surface and the carriers can be modified with aldehyde, succinimidyl ester or amino groups that can react with the amino or thiol groups on the lipase [12].

So far, many types of supporting materials such as activated carbon, graphene, carbon nanotubes, chitosan, silica, metal organic framework, and magnetic nanoparticles were successfully applied to lipase immobilization [12,14–16]. From another point of view, binding the enzyme to a specific support can result in the combination of enzyme-catalyzed reactions with chemical oxidation techniques and enhance the catalytic activities [11,17]. Since the utilization area of immobilized lipases is synchronized with the type and structure of the support material, the development of novel and unique supports plays an important role in the catalytic reactions. The criteria for choosing suitable support material for immobilization generally includes cost-effectiveness, availability, stability and reactivity in specific conditions [9]. In addition, the physicochemical parameters of the support materials that should be taken into account are surface area, particle size, pore structure and type of functional groups present on the surface. Moreover, there should be affinity between the functional groups of the enzyme and supporting material to reduce diffusional limitations and allow the formation of effective binding interactions.

Graphitic carbon nitride (g-C_3N_4), the most stable allotrope of carbon nitride, offers abundant applications in photo-electrocatalysis, sensing, bioimaging and energy conversion processes due to its thermal stability, chemical inertness, electronic structure, and good mechanical properties [18]. The material looks like a cross-linked polymer built from s-triazine or s-heptazine units bonded via secondary or tertiary amino groups [19]. The 2D layered structure of g-C_3N_4 can be easily tuned at the molecular level without changing the composition, which consists of two components abundant on earth (carbon and nitrogen) [20]. The excellent biocompatibility properties and surface-active sites of g-C_3N_4 make it an ideal scaffold for successful enzyme immobilization. The amino groups at the margins of g-C_3N_4 are responsible for forming more stable hybrids via physical or covalent bonding. Hence, it can be hypothesized that g-C_3N_4 will work in a harmony with enzymes. Shen et al. [21] immobilized *Candida rugosa* lipase (CRL) on mesoporous carbon nitride via physical adsorption and achieved improved thermal stability of free CRL. Wang et al. [22] introduced palladium and Candida antarctica lipase B (CalB) immobilized g-C_3N_4 as a new biocatalyst for benzyl hexanoate production and demonstrated that the immobilized CalB had superior performance to the free enzyme. Recently, Li et al. [23] covalently attached Candida rugosa lipase on g-C_3N_4 nanosheets and the immobilized sample had good enzyme-loading, pH-flexibility, and thermostability features. According to these statements, the biocompatibility, low cost, surface-active sites and hydrophobic properties of g-C_3N_4 make it a perfect candidate for lipase immobilization which would further increase the activity of the enzyme. Additionally, the lid opening structure of lipase might be enhanced upon immobilization on the hydrophobic g-C_3N_4. In the physical immobilization process, hydrogen bonding interactions can cause propagation into the distal region which enhances lid opening, while the shift base reactions can improve the lid structure through covalent attachment. In spite of these excellent features, the related literature has rarely reported lipase immobilization on g-C_3N_4, especially in the field of photocatalysis.

Therefore, in this work, we investigated the usage of g-C_3N_4 as a supporting material for immobilization of different lipase enzymes in order to promote both photocatalytic and enzymatic activities. Three lipase enzymes (Palatase 20,000 L, Lipozyme TL100, and Lipozyme CALB) were attached to the g-C_3N_4 structure to form C_3N_4@lipases as biohybrid catalysts via physical adsorption and covalent binding methods. The physical, structural, and optical properties of the biohybrids were explored in detail. The photocatalytic performance of C_3N_4@lipases was investigated by the degradation of tetracycline (TC) and sulfadiazine (SDZ) as model organic pollutants, which commonly exist in the environment and are harmful for living beings.

2. Materials and methods

2.1. Materials

p-nitrophenylpalmitate (p-NPP, Aldrich, 99%), Lipozyme TL 100 L (100,000 U per g solid), Palatase 20,000 L (20,000 U per g solid), and Lipozyme CALB (5,000 U per g solid), absolute ethanol (EtOH), and glutaraldehyde solution (25% (w/v)) were purchased from Sigma-Aldrich (St. Louis, USA). Protein Assay Kit was obtained from Boster Biological Technology (CA, USA). Melamine ($C_3H_6N_6$, 99%) was supplied from Merck. Tetracycline and sulfadiazine were obtained from Sigma-Aldrich. All chemicals were of analytical reagent grade and used as received without any further purification.

2.2. Preparation of graphitic carbon nitride (g-C_3N_4)

The raw graphitic carbon nitride (g-C_3N_4) sample was prepared via thermal decomposition of melamine. The melamine was first heated to 550 ℃ (3 ℃ min^{-1}) in a semi-closed crucible under air and then it was kept at the final temperature for 3 h.

2.3. Immobilization of lipase enzymes on g-C_3N_4

2.3.1. Physical immobilization

The immobilization of Palatase 20,000 L, Lipozyme TL100 L and Lipozyme CALB on g-C_3N_4 was carried out by the physical adsorption method. 0.15 g Palatase 20000L, 0.03 g Lipozyme TL100, and 0.60 g Lipozyme CALB wwere fully dissolved in 50 mL 0.1 M phosphate-buffered saline (PBS,) at pH 7.0. Then, g-C_3N_4 and enzyme solutions were successively mixed, and the mixture was incubated at 25 ℃ in a shaker operating at 140 rpm overnight. The immobilized lipases (C_3N_4@PLTS, C_3N_4@LPZYM, and C_3N_4@-CALB) were collected by refrigerated centrifugation, washed with 0.1 M PBS (pH 7.0) 3 times, freeze-dried overnight, and stored in a refrigerator at 4 ℃.

2.3.2. Covalent immobilization

The immobilization of Palatase 20,000 L, Lipozyme TL100 L and Lipozyme CALB on g-C_3N_4 was performed by the cross-linking method assisted by glutaraldehyde according to literature reports [23]. First, 100 mL 0.1 M PBS buffer (pH 7.0) and 30 mL of glutaraldehyde solution (25%, w/v) were successively added to 250 mL Erlenmeyer flask including 3.0 g of g-C_3N_4. After sonication treatment, the mixture was incubated at 60 ℃ in a shaker operating at 140 rpm overnight. Subsequently, the activated carrier was separated and repeatedly washed with distilled water 3 times via vacuum filtration. Finally, the product was dried in a vacuum oven at 25 ℃ overnight, and the material was named G-g-C_3N_4.

Then, 0.15 g Palatase 20,000 L, 0.03 g Lipozyme TL100 L, and 0.60 g Lipozyme CALB were fully dissolved in 50 mL 0.1 M PBS

(pH 7.0) with mild shaking at 37 ℃. The obtained G-g-C_3N_4 (1.0 g) was dispersed in the lipase solutions which were subsequently incubated at 37 ℃ in a shaker overnight. The immobilized lipases (C_3N_4@PLTS, C_3N_4@LPZYM, and C_3N_4@CALB) were collected by refrigerated centrifugation, washed with 0.1 M PBS (pH 7.0) 3 times, freeze-dried overnight, and stored in a refrigerator at 4 ℃.

2.4. Activity assay and protein determination

The activities of the free and immobilized lipases were measured by the hydrolysis of p-nitrophenol palmitate (p-NPP) in a buffer solution at 37 ℃ for 5 min at 160 rpm. The protein concentrations in C_3N_4@PLTS, C_3N_4@LPZYM, and C_3N_4@CALB were determined by the Bradford method, using bovine serum albumin as standard. The amount of immobilized lipases was calculated by detecting the amount of un-immobilized lipase according to the method described in Li et al. [23].

2.5. Immobilization yield

Immobilization yield was calculated using Eq. (1):

$$\text{Immobilization yield} = \left(\frac{\text{Lipase bound enzyme activity}}{\text{Lipase loading actvity}}\right) \times 100 \quad (1)$$

The activities obtained from other conditions were defined as relative activities, and we assumed the maximum activity value of the immobilized and free lipase under optimal conditions to be 100%.

2.6. Effect of pH and temperature on the immobilization yield

The effects of pH on the activities of free and immobilized lipases were investigated at 37 ℃ at a variety of pHs (5.0, 5.5, 6.0, 6.5, 7.0, 7.5, and 8.0) for 1 h. The effect of temperature on the activities of free and immobilized lipases was investigated at pH 7.0 at different temperatures (30, 40, 50, 60, 70, and 80 ℃) for 1 h. Each treatment was performed in triplicate.

2.7. Characterization

FT-IR spectra were recorded on a Bruker Tensor 27 FT-IR spectrometer with the KBr pellet technique. The crystal phases of samples were measured using a Bruker D8 Advance X-ray diffractometer (Bruker, Germany) with a 2theta range from 10 to 80 with Cu-Ka irradiation. The thermal stabilities of g-C_3N_4, C_3N_4@PLTS, C_3N_4@LPZYM, and C_3N_4@CALB were studied with a thermogravimetric (TGA) analyzer (TAQ50, Netzsch, Germany) at a heating rate of 5 ℃ min^{-1} in a N_2 atmosphere. The morphologies of obtained samples were characterized using a scanning electron microscope operated on 300 kV. The UV–vis absorption spectra were obtained using a diffuse reflectance UV–Vis absorption spectrophotometer (Perkin-Elmer Lambda 750).

2.8. Enzyme kinetics

Hanes Woolf plot is a representation of enzyme kinetics according to the ratio of the initial substrate concentration to the reaction velocity plotted against initial substrate concentration.

$$\frac{[S]}{v} = \frac{1}{V_{max}}[S] + \frac{K_m}{V_{max}} \quad (2)$$

where [S] is the initial pNPP concentration, v is the initial reaction rate, and V_{max} is the maximum velocity of free and immobilized lipases.

2.9. Photocatalytic activity tests

Photocatalytic performances of prepared samples were carried out using a square reactor equipped with two visible lamps (λ: 400–800 nm). A typical degradation test was conducted in suspension including 10 mg of raw g-C_3N_4, C_3N_4@PLTS, C_3N_4@LPZYM, and C_3N_4@CALB and 50 mL of 10 mgL^{-1} pollutant solution at neutral pH of 6.5. Prior to light illumination, the suspension was stirred for 30 min to ensure the equilibrium of adsorption/desorption. During the photocatalytic reaction, aliquots (3 mL) were collected at specific times followed by filtration with a syringe membrane filter. The residual tetracycline (TC) and sulfadiazine (SDZ) concentrations were analyzed by UV–vis absorption spectroscopy at wavelengths of 360 nm and 262 nm, respectively.

The degradation ratio was determined by Eq. (3).

$$X(\%) = \frac{(C_0 - C_t)}{C_0} \times 100 \quad (3)$$

where C_0 and C_t are the concentration before irradiation and after irradiation time t, respectively.

In order to determine the effect of pH, the photo degradation tests of TC and SDZ were evaluated in the presence of C_3N_4@LPZYM catalyst at different pH values, which were adjusted to pH 3.0, 6.5, 8.0, and 13.0. In terms of the scavenger effect, ethylene diamine tetra acetic acid disodium salt (EDTA-2Na, 1.0 mM), isopropyl alcohol (IPA, 1.0 mM), and p-benzoquinone (BQ, 0.1 mM) solutions were applied as scavengers for h^+, •OH, and O_2^-, respectively. Moreover, the effect of co-existing anions was investigated by adding CO_3^{2-}, NO_3^{2-} and SO_4^{2-} anions. Additionally, the thermal stability of the catalyst was examined by increasing ambient temperature to 40 ℃ and 60 ℃. All experiments were performed in duplicate and the average values were reported.

In order to identify the intermediate products with related pathways after TC and SDZ degradation, Perkin Elmer Clarus 580 gas chromatograph equipped with mass spectrometer (GC–MS) was utilized. The solutions were extracted with dichloromethane before analysis.

3. Results and discussion

3.1. Investigation the effect of immobilization method

Since the immobilization method for enzymes directly influences the molecular structure of enzyme and thereby its catalytic activity [13–15], the effect of physical and covalent attachment on the immobilization yield were preliminarily investigated in the present paper. Glutaraldehyde was chosen as cross-linking agent which can be covalently linked between g-C_3N_4 and lipase structures resulting in efficient immobilization through modification of amino groups. It was also reported that the hydrophobicity of g-C_3N_4 could increase by using glutaraldehyde [23].

As shown in Table 1, the immobilization yields were found to be 71.0% and 93.4% for C_3N_4@PLTS; 81.3% and 95.4% for C_3N_4@LPZYM; and 79.4% and 91.7% for C_3N_4@CALB using physical adsorption and covalent bonding methods, respectively. In addition, bound enzyme activities were determined to be 2130 and 2802 U/g g-C_3N_4 for C_3N_4@PLTS; 2559 and 2862 U/g g-C_3N_4 for C_3N_4@LPZYM; and 2382 and 2751 U/g g-C_3N_4 for C_3N_4@CALB using physically and covalently immobilized enzymes, respectively. Lipase immobilization using glutaraldehyde onto g-C_3N_4 showed the highest immobilization yield (95.4%) and the highest activity per gram of carrier (2862 U/g g-C_3N_4) using Lipozyme TL100 L.

The strong conjugate bonds [13] and hydrophobic effect of glutaraldehyde [24] resulted in an efficient immobilization yield through covalent attachment on g-C_3N_4. The surface layers of

Table 1
Immobilization efficiency of lipase enzymes on g-C_3N_4 using physical adsorption and covalent attachment.

Immobilization method	Lipase loading on g-C_3N_4 (U/g)	Bound lipase activity (U/g g-C_3N_4)	Immobilization yield (%)
C_3N_4@PLTS			
Physical immobilization	3000	2130	71.0
Covalent immobilization	3000	2802	93.4
C_3N_4@LPZYM			
Physical immobilization	3000	2559	85.3
Covalent immobilization	3000	2862	95.4
C_3N_4@CALB			
Physical immobilization	3000	2382	79.4
Covalent immobilization	3000	2751	91.7

g-C_3N_4 are decorated with amino groups, while the internal layer consists of heterocyclic carbon–nitrogen aromatic rings [19]. During immobilization, the amino groups of g-C_3N_4 interact with C = O bonds from the aldehyde groups of glutaraldehyde. Then, amide (–CO-NH-) bonds of lipase enzymes attach to the crosslinked group resulting in strong covalent immobilization. In the case of physical adsorption, hydrogen atoms bind to the amino groups of g-C_3N_4. Possible immobilization mechanisms are shown in Fig. 1.

Among the lipase enzymes, Lipozyme TL100L displayed highest immobilization yield for both physical and covalent immobilization methods. Lipozyme TL100L is a 1,3-regioselective and stable lipase. The large hydrophobic pocket surrounding the active site of Lipozyme TL100L might strongly interact with g-C_3N_4. Moreover, the adsorption of Lipozyme TL100L on g-C_3N_4 under different experimental conditions may also affect changes in the shape of the open active center of the enzyme and different activity-selectivity properties of the enzyme.

The influence of immobilization method for Palatase 20000L, Lipozyme TL100L, and Lipozyme CALB enzymes on g-C_3N_4 were also explored for their photocatalytic degradation performances (Fig. 2). In the presence of raw g-C_3N_4, TC degradation was calculated as 52% at the end of 180 min. With the enzyme immobilization, the TC degradation efficiency was significantly accelerated and 69.2%, 83.0% and 98% removal percentages were achieved for physically immobilized C_3N_4@CALB, C_3N_4@PLTS, and C_3N_4@LPZYM biohybrids, respectively. Conversely, lower TC degradation rates were determined as 39.40%, 49.4% and 79.5% for covalently attached Lipozyme CALB, Palatase 20,000 L, and Lipozyme TL 100 L enzymes, respectively. Similarly, SDZ degradation performances increased with enzyme immobilization via physical adsorption on g-C_3N_4; which resulted from the ability of enzymes to enhance the structural and optical properties of the supporting material. The SDZ degradation ratio was found to increase from 43% to 61% with the physically immobilized Lipozyme enzyme. In addition, the photodegradation efficiencies of C_3N_4@CALB and C_3N_4@PLTS were observed to be 50.1% and 57.5%, respectively. For both pollutants, the degradation performances of covalently immobilized biohybrids were lower than physically immobilized ones. Unless the strong crosslinking groups between g-C_3N_4 and glutaraldehyde created new active sites enhancing immobilization yield and biocatalytic activity, these sites dramatically decreased the photocatalytic efficiency of g-C_3N_4 owing to the competitive inhibition of end groups. Therefore, further experiments were conducted with physically immobilized biohybrids and their biocatalytic and photocatalytic behaviors were investigated in detail.

3.2. Characterization of raw g-C_3N_4 and physically immobilized C_3N_4@PLTS, C_3N_4@LPZYM, and C_3N_4@CALB biohybrids

The surface functional groups of raw g-C_3N_4 and physically immobilized C_3N_4@PLTS, C_3N_4@LPZYM, and C_3N_4@CALB biohybrids were investigated by FT-IR (Fig. 3). The bands near 1000 cm^{-1} were assigned to graphitic sp^2 and triazine vibrations. The peak around 800 cm^{-1} was attributed to out-of-plane bending vibration of the H atom on the heptazine ring. The three bands at 1250, 1320, and 1410 cm^{-1} indicated the aromatic C–N stretching of raw g-C_3N_4. The peak at about 1610 cm^{-1} originated from C = N stretching [25], while the peaks between 3000 and 3500 cm^{-1} illustrated the stretching of N-H or terminal NH_2 groups in the aromatic ring of raw g-C_3N_4 [26]. In comparison with raw g-C_3N_4, some differences appeared in the FT-IR spectra with the intensities clearly decreased for C_3N_4@PLTS, C_3N_4@LPZYM, and C_3N_4@CALB biohybrids. The peaks at about 1250, 1320, 1410, and 1610 cm^{-1} seen at lower intensities were assigned to the aromatic C–N and C–N skeleton. These characteristic absorption peaks of C_3N_4@PLTS, C_3N_4@LPZYM, and C_3N_4@CALB highly overlapped with the absorption peaks of g-C_3N_4 due to the physical interaction of lipases with

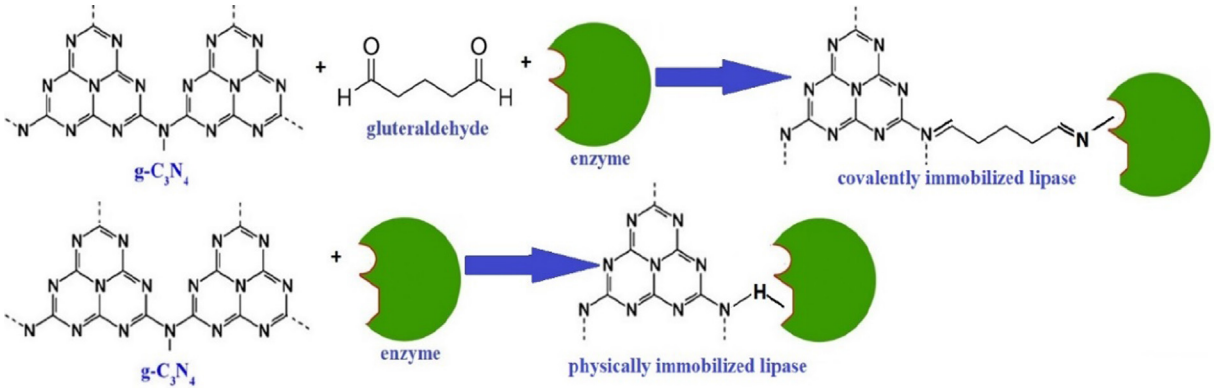

Fig. 1. Immobilization mechanism of physically and covalently immobilized lipase.

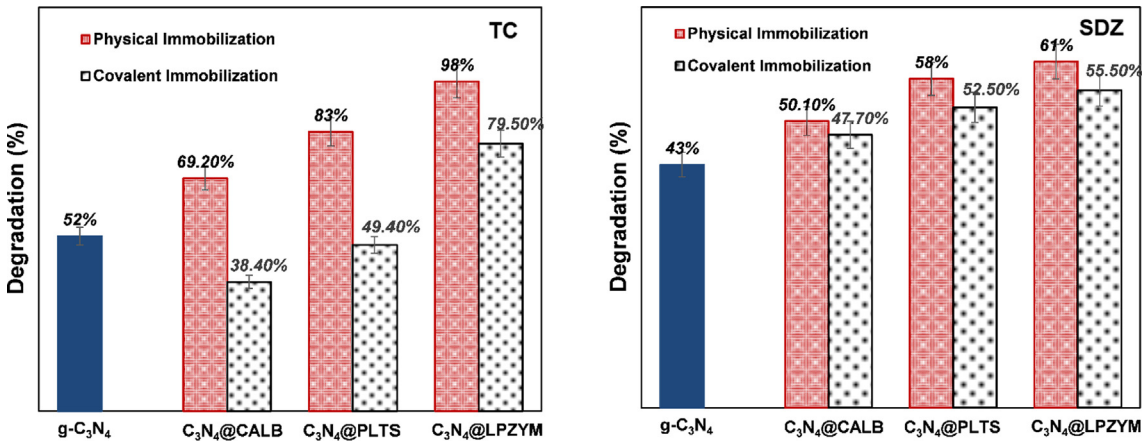

Fig. 2. Effect of immobilization method on the photocatalytic performances of raw g-C_3N_4, C_3N_4@PLTS, C_3N_4@LPZYM, and C_3N_4@CALB.

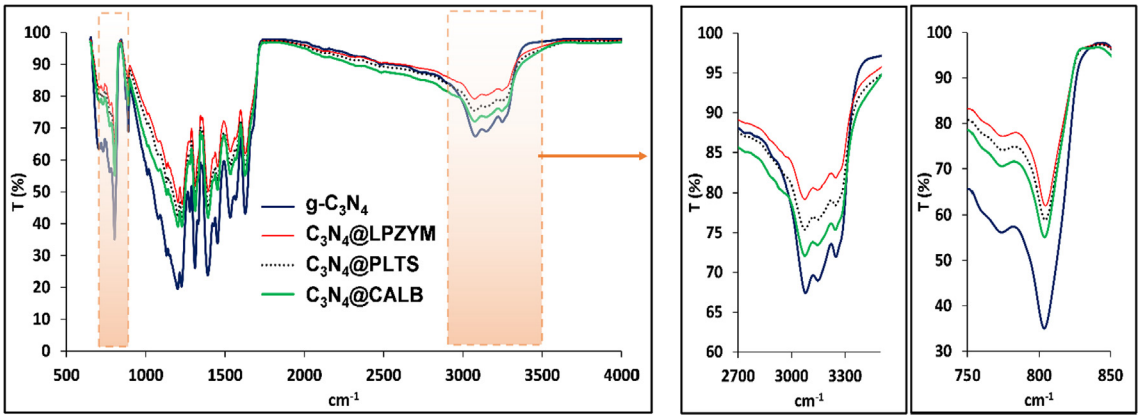

Fig. 3. FT-IR spectrum of raw g-C_3N_4, C_3N_4@PLTS, C_3N_4@LPZYM, and C_3N_4@CALB biohybrids.

the support matrix. The findings revealed that the immobilization process affected the basic surface structure of g-C_3N_4.

Additionally, the most significant difference was determined in the spectra of C_3N_4@LPZYM sample, demonstrating the efficient interaction between Lipozyme TL100L and g-C_3N_4. Comparing the curves of raw g-C_3N_4 and C_3N_4@LPZYM, the N–H and H vibration peaks of g-C_3N_4 at around 3000–3500 and 800 cm^{-1} weakened after immobilization, which can be explained by the successful formation of N–H and H bonds between Lipozyme TL100L and g-C_3N_4. In other words, the amino and carboxylic groups, which are active sites of enzymes, bonded with the surface N–H and H groups resulting in changes in the microenvironment.

The thermal stabilities of raw g-C_3N_4, C_3N_4@PLTS, C_3N_4@LPZYM, and C_3N_4@CALB were characterized by TGA (Fig. 4(a)). The char yields of C_3N_4@PLTS, C_3N_4@LPZYM, and C_3N_4@CALB were nearly same as that of raw g-C_3N_4. All biohybrid catalysts were stable up to about 750 °C, while obvious weight losses of about 4.5% were observed from TGA curves of C_3N_4@PLTS, C_3N_4@LPZYM, and C_3N_4@CALB, respectively. The weight loss beginning from 200 °C was derived from the decomposition of immobilized lipases. In addition, it can be clearly seen from Fig. 4 that lower degradation rates were obtained for C_3N_4@PLTS, C_3N_4@LPZYM, and C_3N_4@CALB in the temperature range of 25 ℃ and 750 ℃. Higher thermal stability with lower degradation rate for biohybrid catalysts could be attributed to the extensive interaction between g-C_3N_4 and lipases.

In Fig. 4(b), the XRD patterns of g-C_3N_4 and C_3N_4@LPZYM biohybrid catalysts were quite different from each other. The characteristic peak at 27.7° was assigned to the graphitic (002) plane of g-C_3N_4. Also, two obvious additional peaks at 2θ of 34.8° and 47.8° were detected in the pattern of C_3N_4@LPZYM. These crystal peaks correspond to the crystalline and/or stereo complex crystals of aspartate, histidine, and serine of all lipases. These features illustrated the typical amino acid/protein phases of enzyme biohybrid catalysts. Furthermore, the XRD pattern of C_3N_4@LPZYM showed a minor peak at 13.2° ascribed to the (100) planes in-planar tris-*s*-triazine of g-C_3N_4. On the other hand, high crystallinity of g-C_3N_4 was observed in the biohybrid sample due to the strong interaction between g-C_3N_4 and Lipozyme TL100L enzyme. This interaction proved the close packaging of g-C_3N_4 molecules required for the formation of regular crystallites.

Scanning electron microscopy (SEM) was carried out to verify the surface morphology of g-C_3N_4 and C_3N_4@PLTS, C_3N_4@LPZYM, and C_3N_4@CALB (coded as C_3N_4@Lipases in the figure) (Fig. 5). The raw g-C_3N_4 had a lamellar, non-homogenous, and porous surface structure with wrinkles. The particle size of synthesized g-C_3N_4 were below 100 μm in diameter. Also, non-homogenous internal structure of raw g-C_3N_4 was obvious in the high magnification SEM image. Meanwhile, C_3N_4@Lipases displayed smooth layers which were attributed to the immobilized lipase layer. These observations demonstrated successful immobilization of lipases onto the g-C_3N_4 structure.

In Fig. 6, the UV–vis absorption curves showed that both raw g-C_3N_4 and lipase immobilized g-C_3N_4 biohybrids absorbed a considerable amount of visible light and in turn have potential for use as visible-light-driven photocatalysts. The corresponding band gap

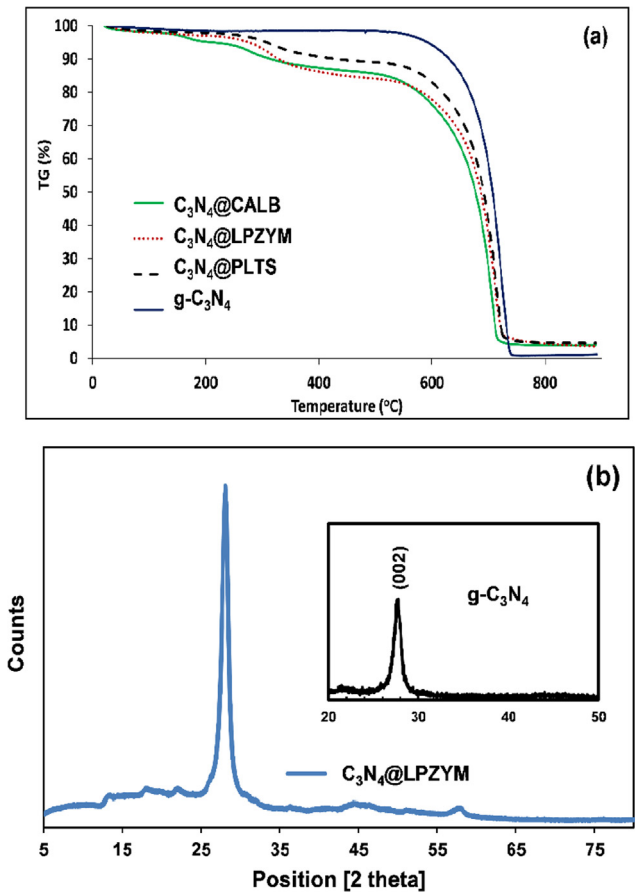

Fig. 4. (a) TGA and (b) XRD results for samples.

energies of g-C_3N_4, C_3N_4@PLTS, C_3N_4@LPZYM, and C_3N_4@CALB were 2.75 eV, 2.70 eV, 2.6 eV and 2.6 eV, respectively (Fig. 5(b)). Of note, such a decrease in band gap energy value suggests enhanced potential for visible light activation, enabling these biohybrids to be promising candidates for photocatalytic applications.

3.3. Biocatalytic activities of biohybrids

To investigate the biocatalytic applications of C_3N_4@PLTS, C_3N_4@LPZYM, and C_3N_4@CALB samples, the enzyme activities were determined using the hydrolysis reaction of p-NPP. It was foreseen that the interactions between lipase enzymes and triazine rings of g-C_3N_4 might increase the catalytic activity of lipases, thus enhancing the enzymatic activity of the hydrolysis of substrate molecules at active sites.

Since pH of solution and temperature seriously affect the relative activities of free and immobilized lipases when hydrolyzing p-NPP, the effects of these parameters were investigated, and the results are presented in Fig. 7(a). Compared to the free Palatase 20000L, Lipozyme TL100 L, and Lipozyme CALB (pH 7.0, 7.0, and 5.0, respectively), the optimum pH of C_3N_4@PLTS, C_3N_4@LPZYM and C_3N_4@CALB shifted toward the basic region (pH 7.5, 7.5, and 6.5, respectively). This shift could be associated with the conformational variation of enzyme on the support and protonation of the micro-environment. When the free lipase enzymes directly accessed the substrate in soluble form, the $-NH_2$ groups on the g-C_3N_4 might stabilize the pH of the microenvironment surrounding the enzyme, thereby affecting the protonation of the protein molecule [27]. Meanwhile, the enzyme activity of C_3N_4@PLTS, C_3N_4@LPZYM and C_3N_4@CALB biohybrids showed better performance when the pH was changed from 5.0 to 8.0, which demonstrated improved stability in comparison to the free form. It could be speculated that the integrity of Palatase 20000L, Lipozyme TL100 L, and Lipozyme CALB enzymes was preserved over a wider pH range by immobilization on the g-C_3N_4 matrix. A similar approach was stated about Candida antarctica lipase B which displayed an enhanced catalytic rate when it was adsorbed on a hydrophobic interface and it was demonstrated that the increased activity was due to the conformational changes in open active sites [2].

As shown in Fig. 7(b), C_3N_4@PLTS, C_3N_4@LPZYM and C_3N_4@CALB biohybrid catalysts exhibited better relative enzyme activities than their free forms in the range from 30 ℃ to 40 ℃. Due to denaturation, the relative activity of the free lipases decreased rapidly when there was an increase in temperature (0% of initial activity at 70 ℃ and 80 ℃). In contrast, the immobilized lipases were more heat-resistant than the free lipases at higher temperatures. This might

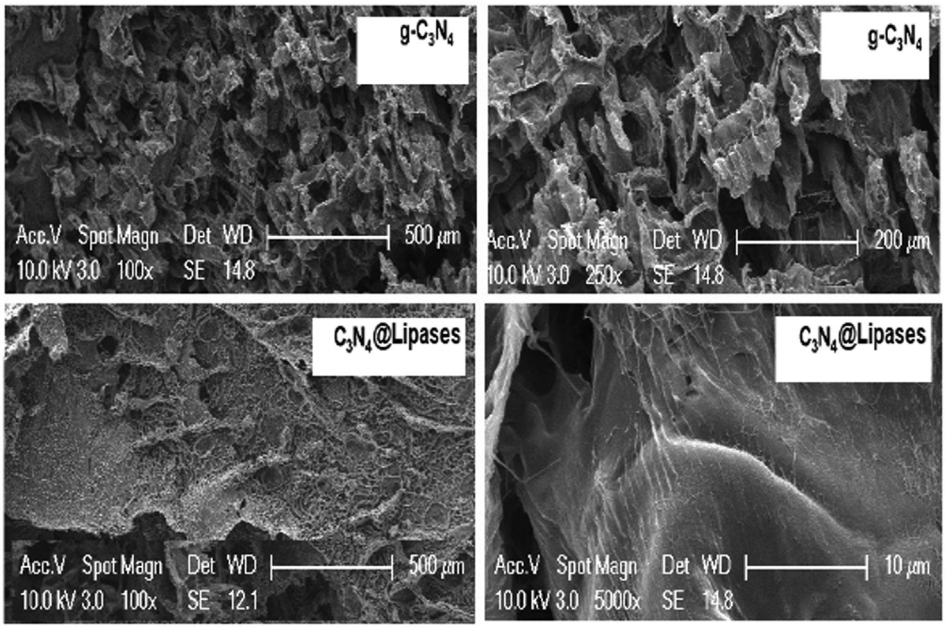

Fig. 5. SEM images of g-C_3N_4, C_3N_4@PLTS, C_3N_4@LPZYM, and C_3N_4@CALB (coded as C_3N_4@Lipases in the figure) (x100 and x5000).

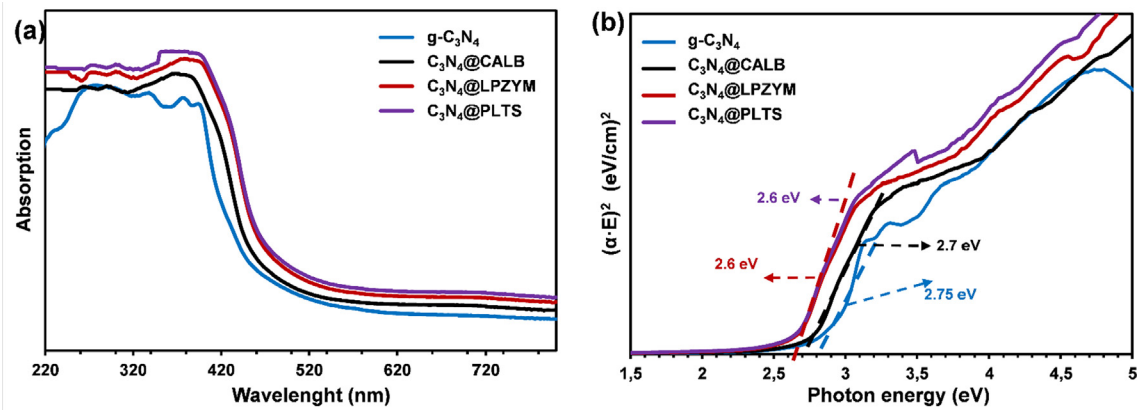

Fig. 6. (a) UV–vis absorption spectra (b) Kubelka-Munk function for raw g-C_3N_4, C_3N_4@PLTS, C_3N_4@LPZYM, and C_3N_4@CALB biohybrids.

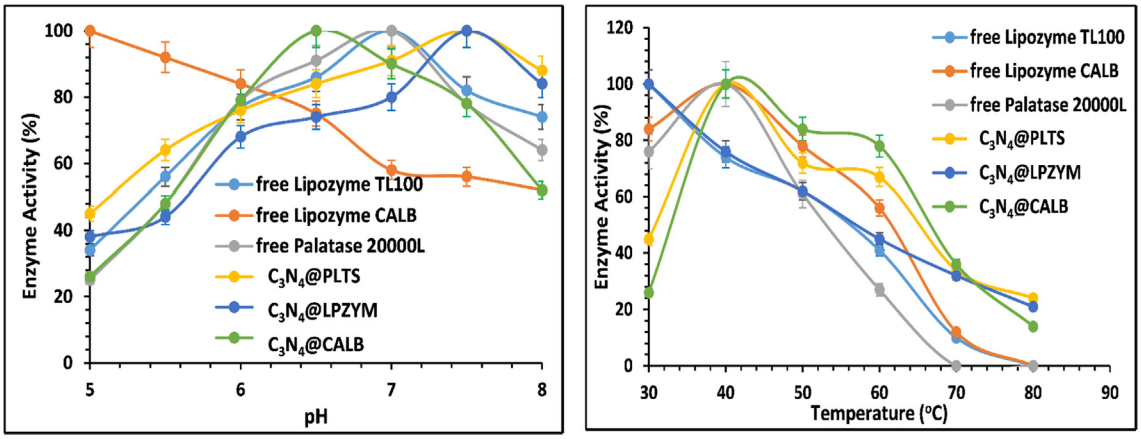

Fig. 7. Effects of (a) pH and (b) temperature on the activities of free and physically immobilized lipases.

be explained by the formation of chemical bonds during the physical bonding process, which could effectively restrict the conformation distortion or damage during periods of elevated temperature. Analogous results were obtained by other researchers for lipase immobilization, as summarized in Table S1.

3.3.1. Kinetic studies

Kinetic parameters (K_m and V_{max}) for free and physically immobilized lipases were determined using Hanes Woolf model at optimum pH and room temperature. The immobilization process changed the K_m and V_{max} values of free Lipozyme TL 100 L, Palatase 20,000 L, and Lipozyme CALB enzymes (Table 2).

V_{max} and K_m values of immobilized Palatase 20,000 were determined to be 5.81 μMmin^{-1} and 81.39 mM, respectively, compared to free enzyme values of 3.73 μMmin^{-1} and 55.23 mM. Additionally, V_{max} and K_m values of immobilized Lipozyme CALB were found to be 2.13 μMmin^{-1} and 36.6 mM compared to free enzyme values of 3.42 μMmin^{-1} and 19.83 mM respectively. K_m and V_{max} values of immobilized Lipozyme TL100L were calculated to be 71.5 mM and 1.77 μMmin^{-1} compared to free enzyme values of 4.2 mM and 1.75 μMmin^{-1}. As is known, K_m represents the enzyme affinity; higher values of K_m represent higher affinity of the enzyme [28]. In other words, high K_m values indicate how efficiently an enzyme selects its substrate and converts to product. In this study, the increment in all K_m values after the immobilization process indicates the increase in enzyme affinity. K_m values of Lipozyme TL 100 L increased 17 fold after immobilization. The K_m value of the immobilized Lipozyme TL 100 L, 71.5 mM, was higher than the K_m of the free one, 4.2 mM; revealing that the immobilized enzyme needs a higher concentration of substrate. This situation represents higher mass transfer resistance, steric hindrance, enzyme conformational changes, and limited accessibility to the enzyme active sites [29]. These findings confirmed the successful attachment of all enzymes to the g-C_3N_4 surface.

The maximum reaction velocity (V_{max}) values for the immobilized Lipozyme TL 100 L, Palatase 20,000 L, and Lipozyme CALB were determined. It was found that V_{max} values decreased from 1.77 to 1.75 μmol min^{-1} for Lypozyme TL 100 L and 5.81 to 3.73 μmol min^{-1} for Palatase 20,000 L, respectively. These data showing higher K_m value with lower V_{max} value for physically immobilized lipases agree with the findings of Kashefi et al. [29].

Table 2
Kinetic parameters of free and physically immobilized Lipozyme TL 100 L, Palatase 20,000 L, and Lipozyme CALB enzymes.

Enzyme form	K_m (mM)	V_{max} (μM.min^{-1})
C_3N_4@PLTS		
Free	55.23	3.73
Physical immobilization	81.9	5.81
C_3N_4@LPZYM		
Free	4.20	1.75
Physical immobilization	71.5	1.77
C_3N_4@CALB		
Free	19.83	3.42
Physical immobilization	36.60	2.13

3.4. Photocatalytic degradation studies

Photocatalytic performance of raw and enzyme immobilized g-C_3N_4 was also investigated towards pharmaceuticals, namely tetracycline (TC) and sulfadiazine (SDZ), under visible light irradiation and the results are illustrated in Fig. 8. In order to examine the role of adsorption in the removal performance, the preliminary control experiments were conducted in the dark and the results are presented in the inset of Fig. 8. The raw g-C_3N_4 itself adsorbed 21% of TC in the dark adsorption period. The introduction of enzymes into the g-C_3N_4 structure favors a slight improvement in the TC adsorption performance and about 29%, 27% and 32% adsorptive removal rates were observed for C_3N_4@CALB, C_3N_4@PLTS, and C_3N_4@LPZYM samples, respectively. This reveals the fact that adsorption might play a minor role in the degradation efficiency of TC. On the other hand, different from TC removal, the SDZ adsorption efficiency of raw g-C_3N_4 was very low, calculated as 3.0% at the end of 3 h. After the immobilization of Lipozyme CALB, Palatase 20000L, and Lipozyme TL100L enzymes, 9.4%, 14.3% and 14.4% of SDZ adsorption rates were calculated indicating that SDZ degradation could be mainly enhanced due to the catalytic degradation. In general, the immobilized enzymes cannot significantly oxidize or adsorb the tested antibiotics demonstrating that enhanced visible light absorption properties of biohybrid catalysts might be more dominant for photocatalytic performance.

The photodegradation experiments revealed that the enzyme immobilization on the g-C_3N_4 structure significantly improved the TC degradation performance with removal percentages increasing from 52% to 98%, while the SDZ degradation ratio increased from 42.5% to 60.5% for the C_3N_4@LPZYM sample. Among the immobilized lipase enzyme types, the Lipozyme TL100L enzyme attached to g-C_3N_4 exhibited the best photocatalytic performance for both antibiotics. The difference in the photocatalytic activities could be ascribed to the structural and functional differences between the studied lipase enzyme types. Researchers demonstrated that the amino acid sequence and lid configurations of lipases play important roles in the catalytic activity and specificity [15]. The lid of the lipase enzyme reflects to its amphipathic structure, in which the hydrophilic side faces the solvent in the closed form, while the hydrophobic side is exposed to the catalytic site [2]. When the lid is closed, it enables the active site to face towards substrate and the lipase will be inactive; while in open conformation, substrates can reach active sites [30]. It can be stated that lipases with similar lid configuration or flexibility might have similar immobilization efficiency. Lipozyme TL100L is a specific lipase and shows high substrate selectivity to large side chains/large groups. Additionally, Lipozyme TL100L has the highest open lid and large hydrophobic pocket surrounding the active site among the other selected enzymes; thus, the highest photocatalytic activity could be obtained with C_3N_4@LPZYM biohybrid catalyst. Considering these results, subsequent experiments were conducted with C_3N_4@LPZYM as the best catalyst.

The degradation performances of the enzyme immobilized catalysts were further evaluated based on the Langmuir-Hinshelwood

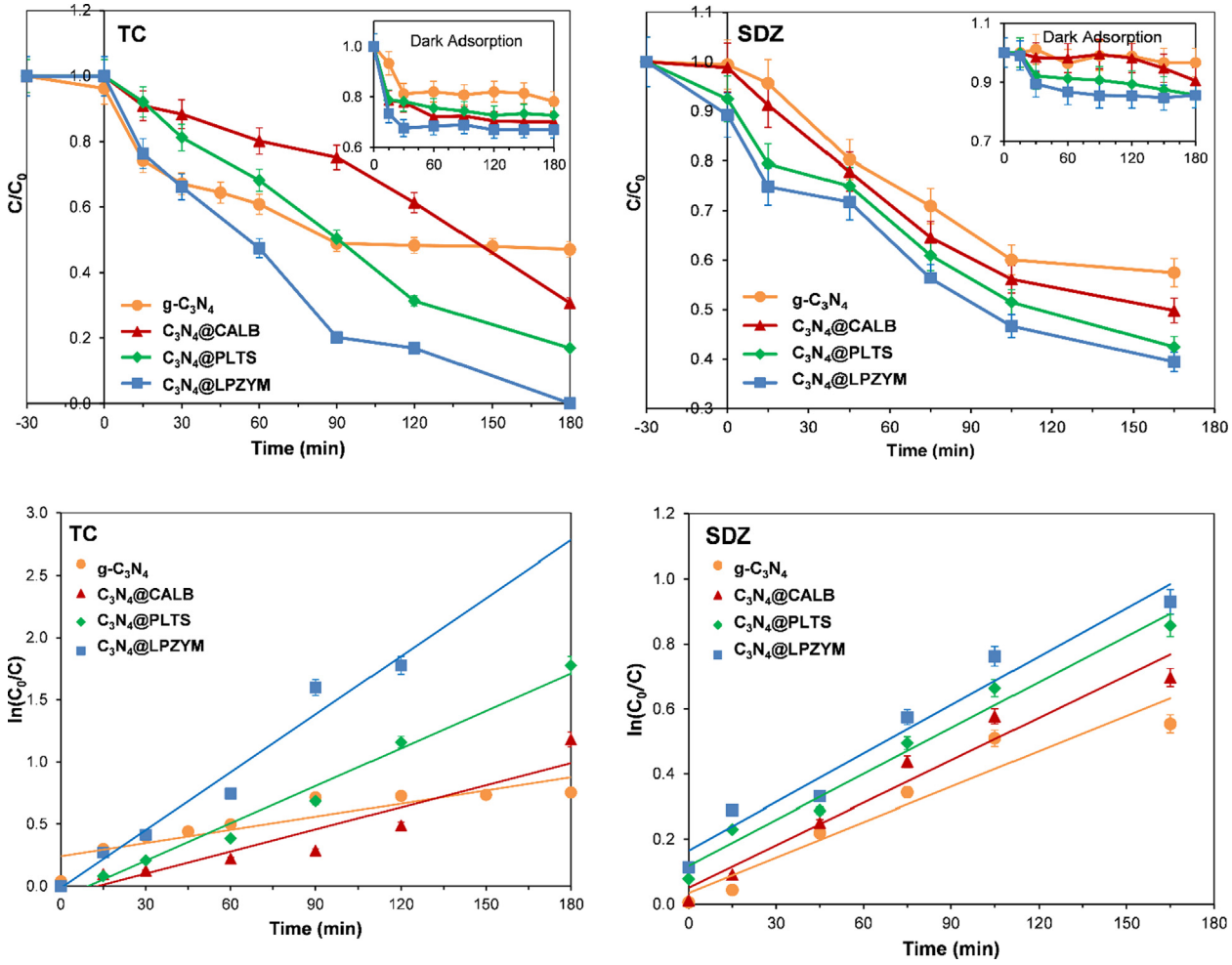

Fig. 8. Photocatalytic degradation performances of raw g-C_3N_4, C_3N_4@PLTS, C_3N_4@LPZYM, and C_3N_4@CALB (Inset shows the dark adsorption performances of samples).

kinetic model. According to the linear plots of the pseudo-first-order kinetic model (Fig. 8), both TC and SDZ degradation by the synthesized biohybrids satisfied the requirements for pseudo-first-order kinetics ($\ln(C/C_0) = k_{app}t$). The apparent reaction rate constants (k_{app}) of raw g-C_3N_4 were calculated as $0.35x10^{-2}$ min^{-1} and $0.27x10^{-2}$ min^{-1} for TC and SDZ degradations, respectively. The Lipozyme TL100 immobilized g-C_3N_4 catalyst possessed higher degradation rate constants for TC (k_{app} = $3.73x10^{-2}$ min^{-1}) and SDZ degradation (k_{app} = $0.44x10^{-2}$ min^{-1}) than for raw g-C_3N_4.

Compared with tetracycline antibiotic, the sulfadiazine degradation performances of both raw g-C_3N_4 and lipase immobilized catalysts were lower, indicating that it is a more recalcitrant pollutant. It is known that the sulfonamide groups exhibit strong chemical stability and solubility in aqueous media; thereby, the rapid and complete degradation of these groups are an important issue and effective techniques are needed [31]. The decomposition pathway of SDZ could begin by breaking the pyrimidine ring that is a feature of high chemical stability; while the TC degradation mechanism is generally proposed as open-ring reactions and further oxidation of byproducts into small organic acids [32]. These phenomena might explain the lower photodegradation of SDZ than TC. Similar phenomena were observed by Garcia-Delgado et al. [33] who explored the biocatalytic removal of tetracycline and sulfonamide via mediator-assisted laccase oxidation. Ding et al. [34] demonstrated that the K_d values were important for the removal of antibiotics. They underlined that tetracycline could be easily adsorbed due to high K_d values, whereas the K_d of sulfonamides were relatively low. Accordingly, these assumptions can explain the difference in the adsorption and photocatalytic removal rates for TC and SDZ antibiotics.

3.4.1. Effect of solution pH

Since the solution pH affects the generation of hydroxyl radicals and also influences the surface charge and interface potential properties of the catalyst, it is one of the important factors in the photocatalytic degradation. Therefore, the effect of solution pH on the performance of C_3N_4@LPZYM catalyst for the TC and SDZ degradation were evaluated in the pH range of 3.0 and 13.0. When the solution pH was adjusted to pH 3.0, almost complete TC degradation was observed within 120 min, while 98% and 80% of TC were degraded at pH 6.5 and 8.0, respectively. This indicates that the catalysts can exhibit ideal performance in a range of pH from 3.0 to 8.0 (Fig. 9(a)). On the other hand, almost no catalytic degradation was observed at pH 13. These findings may be related with both enzyme properties and pK_a characteristics of tetracycline. The pK_a values of TC are 3.3, 7.7, 9.7 and 12.0, which results in different chemical states at these pH values as: (i) H_4TC^+ (pH < 3.3), (ii) H_3TC (3.3 < pH < 7.7), (iii) H_2TC^- (7.7 < pH < 9.7) and (iv) HTC^{2-} (pH > 12) [35]. Accordingly, at higher pH values, the repulsion forces might be dominant between HTC^{2-} and the negatively-charged catalyst surface, limiting the photocatalytic removal. Besides, SDZ degradation reached maximum photocatalytic efficiency at pH 8.0 (75.1% degradation), while it reduced at pH 3.0 (31.3% degradation) and 13.0 (40.1% degradation). According to the pK_a values of SDZ (1.8 and 5.7) [34], at lower pHs than 5.7, electrostatic repulsion forces might occur between the protonated CNH_2 and C_2NH groups on the g-C_3N_4 surface and SDZ^+ molecules; thereby, lower degradation efficiency was observed.

3.4.2. Effect of co-existing anions

It is well-known that the presence of co-existing anions strongly affects the removal efficiency of pollutants in industrial wastewater treatment. Especially, in catalytic removal processes, the anions act as free radical scavengers and produce anion reactive species [36]. Therefore, the effects of co-existing inorganic anions on TC and SDZ degradation performance of C_3N_4@LPZYM were investigated by adding SO_4^{2-}, NO_3^- and CO_3^{2-} (0.1 M) into the suspension and the results are depicted in Fig. 9(b). The addition of sulfate caused a slight depression in the TC degradation (86.5% removal), while the presence of carbonate significantly decreased the TC removal from 98% to 58.3%.

Unlike TC degradation, the presence of sulfate anions had no inhibitory effect on SDZ degradation. Luna et al. [37] underlined the fact that the sulfate anions could react with photo induced holes producing oxidizing radicals and promoting •OH formation by reacting with H_2O molecules resulting in enhanced photocatalytic degradation. On the other hand, SDZ removal was inhibited in the presence of nitrate (49.6% removal) and carbonate (38.3% removal) as the anions served as radical scavengers and prevented radical formation (Eqs. 4–6).

The decrease may also be related to the coverage of active surface sites on the catalysts by anions, reducing the number of surface-active sites [36].

$$CO_3^{2-} + HO\bullet \rightarrow CO_3^{\bullet -} + OH^- \quad (4)$$

$$2CO_3^{\bullet -} + H_2O \rightarrow 2CO_2 + HO_2^- + OH^- \quad (5)$$

$$NO_3^- + HO\bullet \rightarrow NO_3^{\bullet} + OH^- \quad (6)$$

3.4.3. Effect of reactive oxidative species

The trapping experiments were carried out in order to explore the involvement of reactive oxidative species in the TC and SDZ photodegradation with the C_3N_4@LPZYM biohybrid catalyst. For this purpose; isopropyl alcohol (IPA), benzoquinone (BQ) and EDTA-2Na were added to trap the generated hydroxyl radicals (•OH), superoxide radicals ($\bullet O_2^-$) and holes (h^+), respectively. As seen in Fig. 9(c), TC degradation decreased from 98% in the absence of scavenger to 79% upon addition of IPA, indicating the minor role of hydroxyl radicals. Additionally, with the addition of EDTA-2Na and BQ, the degradation efficiencies significantly reduced to 38.3% and 16.8%, respectively. Similarly, the SDZ photodegradation was sharply decreased upon the addition of BQ, implying that the superoxide radicals were the predominant reactive species in the degradation process for both antibiotics.

3.4.4. Effect of temperature on the photodegradation performance of biocatalysts

Since the catalytic properties of the enzymes can be influenced by temperature, the photodegradation performances of C_3N_4@LPZYM catalyst for tetracycline and sulfadiazine removal were investigated in a range of temperatures from 25 °C to 60 °C. From the results shown in Fig. 10, for both antibiotics, the highest removal efficiencies were observed at 25 °C; while the slight decrease with increasing temperature revealed the thermal stability of the C_3N_4@LPZYM enzyme.

With the increase in temperature from 25 °C to 60 °C, the TC degradation slightly decreased from 98% to 75% at the end of 3 h. Similarly, the SDZ degradation rates were calculated as 60%, 57% and 54% at temperatures of 25 °C, 40 °C and 60 °C, respectively. This decreasing trend could be ascribed to the properties of C_3N_4@LPZYM, which exhibits maximum activity in the temperature range 30–60 °C. Since free enzymes can be unstable above ambient temperatures, the slight decrease in degradation could be the result of the formation of stable and strong interaction of lipase on the carbon nitride surface. Similar phenomena were reported by Zdarta et al. [38], who examined the biocatalytic degradation of tetracycline on laccase immobilized electrospun nanofibers.

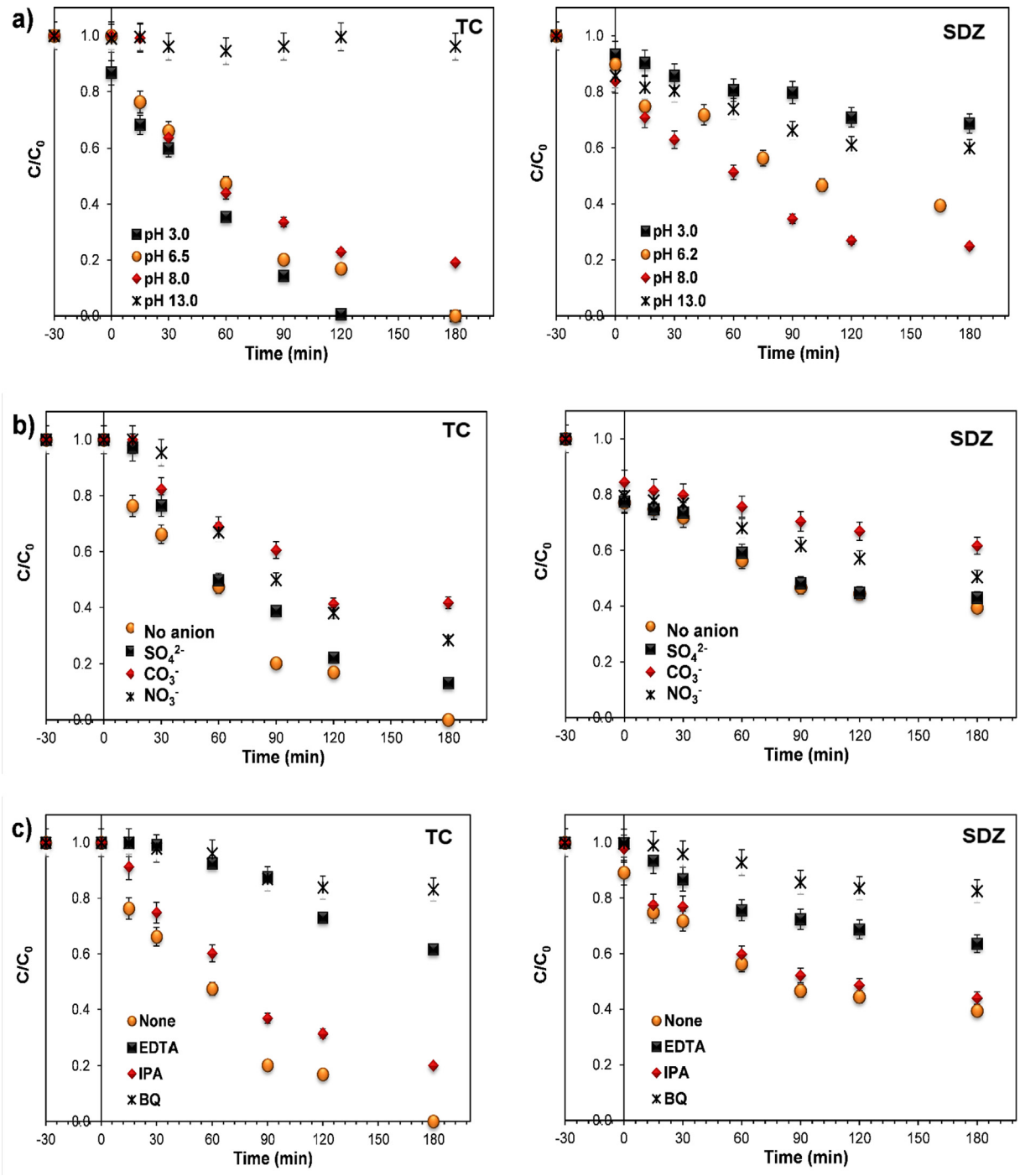

Fig. 9. Effects of solution pH (a), co-existing anions (b) and reactive oxidative species (c) on the photocatalytic degradation of TC and SDZ.

3.5. Photodegradation pathways of target molecules

The degradation products of TC and SDZ were identified by gas chromatography coupled with mass spectrometer, and degradation pathways are shown in Fig. 11. The EI mass spectra of the intermediate products are indicated on Figs. S1-S2. The tetracycline degradation might have occurred via two possible degradation pathways. In *Pathway I*, a product with *m*/*z* of 464 could be formed through radical attack which breaks C = C bonds of tetracycline (*m*/*z* = 445). It was suggested that the electrophilic $\bullet O_2^-/^1O_2$ radicals firstly attacked the TC molecule leading to the formation of intermediates with *m*/*z* ~ 464 accompanied with epoxide and singlet oxygen followed by partial breakage of the double C–C bond [39]. The intermediate with *m*/*z* of 392 was attributed to the breaking of amido and amino groups which subsequently degraded to a product with *m*/*z* of 306 via oxidation and ring opening reactions [40]. After losing methyl groups on the carbon atom ring, the intermediate product with *m*/*z* of 278 was formed while alcohols and acids were broken on the carbocycle resulting in the formation of a product with *m*/*z* of 230. In case of *Pathway II*, the product with *m*/*z* of 355 could form via breakage of -N-CH_3 group followed by loss of amino and acylamino groups [41]. Further degradation led to its demethylation and formation of a corresponding product with *m*/*z* of 281. Afterwards, the aromatic com-

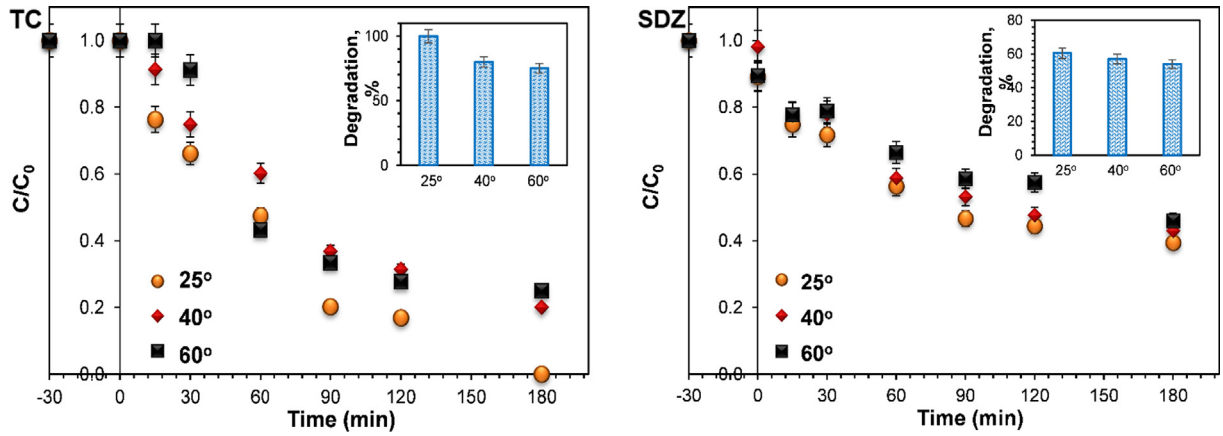

Fig. 10. Effect of temperature on the photocatalytic degradation of TC and SDZ.

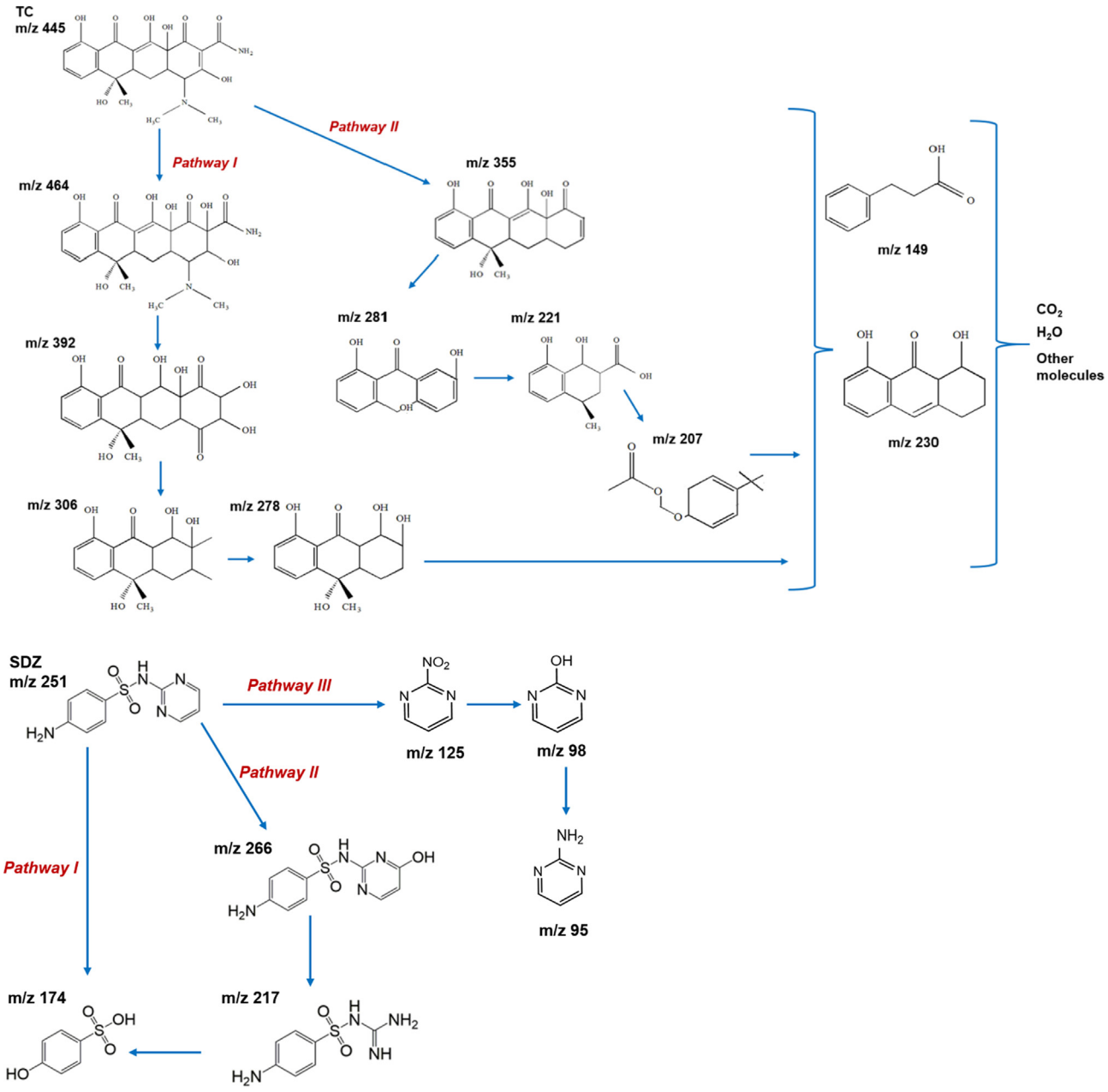

Fig. 11. Proposed degradation pathway for selected molecules with C_3N_4@LPZYM biohybrid catalyst.

pounds with smaller *m*/*z* values of 221, 207, and 149 were released through oxidation reactions [40,42]. Eventually, all products were further mineralized into CO2, H2O and other small molecules.

For the photodegradation of SDZ, intermediate products with *m*/*z* of 95, 174, 266 were detected and the corresponding MS spectra are presented in Fig. S2**.** According to the detected products, three pathways were proposed. In *Pathway I*, the sulfadiazine molecule was destroyed through the cleavage of the S–N bond resulting in formation of and intermediate with *m*/*z* of 174 (p-aminobenzene sulfonic acid) [43]. In terms of Pathway II, the formation of the product (*m*/*z* 266) could be attributed to the •OH radicals which caused hydroxylation reactions on the benzene ring of SDZ [43,44]. Then, C–N breakage might occur generating a product with *m*/*z* of 217. After opening of heterocyclic rings and the cleavage of S–N and C–N bonds, the products might be decomposed to the intermediate with *m*/*z* 174. In the third photodegradation pathway, the sulfadiazine molecule might degrade to the intermediate with *m*/*z* of 125 (2-nitropyrimidin) by breaking the pyrimidine ring which subsequently transformed to pyrimidine molecules with *m*/*z* 96 (1H-pyrimidin-2-one) and *m*/*z* 95 (2-aminopyrimidine) [45].

4. Conclusion

In this work, a green approach was developed for enhanced biocatalytic and photocatalytic performance by utilizing graphitic carbon nitride as a new platform for the immobilization of lipase enzymes. The synthesized biocatalysts showed high enzyme activity as well as thermal stability and pH tolerance. The enzyme activity of immobilized lipase species showed better performance when the pH was changed from 5.0 to 8.0, when compared to the free form. The photocatalytic activities were investigated for the degradation of two antibiotics and the results showed that the biohybrids yielded higher photodegradation rates which was ascribed to the narrow band gap energy and hydrophilic properties of g-C_3N_4. The trapping experiments of active species demonstrated that the hydroxyl radicals and holes were the main active species accounted for the TC degradation, while $\bullet O_2^-$ radicals were dominant for SDZ removal. This study revealed that C_3N_4@lipases are a promising biomimetic photocatalytic material for the degradation of environmental pollutants in an ecofriendly way. Also, g-C_3N_4 can be considered for immobilizing more types of enzymes which will be important in guiding the development of multifunctional catalysts both in enzymatic and photocatalytic processes.

CRediT authorship contribution statement

Esra Bilgin Simsek: Conceptualization, Methodology, Investigation, Data curation, Visualization, Writing - original draft, Writing - review & editing. **Didem Saloglu:** Conceptualization, Methodology, Investigation, Data curation, Writing - original draft, Writing - review & editing.

Declaration of Competing Interest

The authors declare that they have no known competing financial interests or personal relationships that could have appeared to influence the work reported in this paper.

Acknowledgement

The authors thank Ozlem Tuna for kind help with carbon nitride synthesis.

Appendix A. Supplementary data

Supplementary data to this article can be found online at https://doi.org/10.1016/j.molliq.2021.116612.

References

[1] S. Aggarwal, A. Chakravarty, S. Ikram, A comprehensive review on incredible renewable carriers as promising platforms for enzyme immobilization & thereof strategies, Int. J. Biol. Macromol. In press, https://doi.org/10.1016/j.ijbiomac.2020.11.052.
[2] F.I. Khan, D. Lan, R. Durrani, W. Huan, Z. Zhao, Y. Wang, The Lid Domain in Lipases: Structural and Functional Determinant of Enzymatic Properties, Front. Bioeng. Biotechnol. 5 (2017) 16, https://doi.org/10.3389/fbioe.2017.00016.
[3] C. Ortiz, M.L. Ferreira, O. Barbosa, J.C.S. dos Santos, R.C. Rodrigues, A. Berenguer-Murcia, L.E. Briand, R. Fernandez-Lafuente, Novozym 435: the "perfect" lipase immobilized biocatalyst, Catal. Sci. Technol. 9 (2019) 2380, https://doi.org/10.1039/c9cy00415g.
[4] M. Lotti, L. Alberghina, Chapter 16 Lipases: Molecular Structure and Function, J. Polaina and A.P. MacCabe (eds.), Industrial Enzymes, pp. 263–281. Springer (2007) https://doi.org/10.1007/1-4020-5377-0_16.
[5] L. Polgár, The catalytic triad of serine peptidases, CMLS 62 (2005) 2161–2172, https://doi.org/10.1007/s00018-005-5160-x.
[6] R. Fernandez-Lafuente, Lipase from Thermomyces lanuginosus: Uses and prospects as an industrial biocatalyst, J. Mol. Catal. B Enzym. 62 (2010) 197–212. https://doi:10.1016/j.molcatb.2009.11.010.
[7] M.A. Maria-Solano, E. Serrano-Hervás, A. Romero-Rivera, J. Iglesias-Fernández, S. Osuna, Role of conformational dynamics in the evolution of novel enzyme function, Chem. Commun. 54 (2018) 6622–6634, https://doi.org/10.1039/C8CC02426J.
[8] W. Zhou, W. Zhang, Y. Cai, Laccase immobilization for water purification: A comprehensive review, Chem. Eng. J. 403 (2021), https://doi.org/10.1016/j.cej.2020.126272 126272.
[9] J. Zdarta, A.S. Meyer, T. Jesionowski, M. Pinelo, Review : A General Overview of Support Materials for Enzyme Immobilization: Characteristics, Properties, Practical Utility, Catalysts 8 (2018) 92, https://doi.org/10.3390/catal8020092.
[10] T. Jesionowski, J. Zdarta, B. Krajewska, Enzyme immobilization by adsorption: a review, Adsorption 20 (2014) 801–821, https://doi.org/10.1007/s10450-014-9623-y.
[11] C. Ding, J. Liang, Z. Zhou, Y. Li, Wenchao Peng, Guoliang Zhang, Fengbao Zhang, Xiaobin Fan Photothermal enhanced enzymatic activity of lipase covalently immobilized on functionalized $Ti_3C_2T_X$ nanosheets, Chem. Eng. J. 378 (2019), https://doi.org/10.1016/j.cej.2019.122205 122205.
[12] A.R. Ismail, K.H. Baek, Lipase immobilization with support materials, preparation techniques, and applications: Present and future aspects, Int. J. Biol. Macromol. 163 (2020) 1624–1639, https://doi.org/10.1016/j.ijbiomac.2020.09.021.
[13] L. Zhong, Y. Feng, G. Wang, Z. Wang, M. Bilal, H. Lv, S. Jia, J. Cui, Production and use of immobilized lipases in/on nanomaterials: A review from the waste to biodiesel production, Int. J. Biol. Macromol. 152 (2020) 207–222, https://doi.org/10.1016/j.ijbiomac.2020.02.258.
[14] S.E. Collins, V. Lassalle, M.L. Ferreira, FTIR-ATR characterization of free Rhizomucor meihei lipase (RML), Lipozyme RM IM and chitosan-immobilized RML, J. Mol. Catal. B Enzym. 72 (2011) 220–228, https://doi.org/10.1016/j.molcatb.2011.06.009.
[15] J. Mulinari, J.V. Oliveira, D. Hotza, Lipase immobilization on ceramic supports: An overview on techniques and Materials, Biotechnol. Adv. 42 (2020), https://doi.org/10.1016/j.biotechadv.2020.107581 107581.
[16] Z. Ashkan, R. Hemmati, A. Homaei, et al., Immobilization of enzymes on nanoinorganic support materials: An update, Int. J. Biol. Macromol. xxx (xxxx) xxx. https://doi.org/10.1016/j.ijbiomac.2020.11.127.
[17] M. Bilal, S.S. Ashraf, D. Barceló, H.M.N. Iqbal, Biocatalytic degradation/redefining "removal" fate of pharmaceutically active compounds and antibiotics in the aquatic environment, Sci. Total Environ. 691 (2019) 1190–1211, https://doi.org/10.1016/j.scitotenv.2019.07.224.
[18] T.O. Ajiboye, A.T. Kuvarega, D.C. Onwudiwe, Graphitic carbon nitride-based catalysts and their applications: A Review, Nano-Struct. Nano-Objects 24 (2020), https://doi.org/10.1016/j.nanoso.2020.100577 100577.
[19] M. Fronczak, Adsorption performance of graphitic carbon nitride-based materials: Current state of the art, J. Environ. Chem. Eng. 8 (2020), https://doi.org/10.1016/j.jece.2020.104411 104411.
[20] K.R. Reddy, C.H.V. Reddy, M.N. Nadagouda, N.P. Shetti, S. Jaesool, T.M. Aminabhavi, Polymeric graphitic carbon nitride (g-C_3N_4)-based semiconducting nanostructured materials: Synthesis methods, properties and photocatalytic applications, J. Environ. Manage. 238 (2019) 25–40, https://doi.org/10.1016/j.jenvman.2019.02.075.
[21] W. Shen, L. Ren, H. Zhou, S. Zhang, W. Fan, Facile one-pot synthesis of bimodal mesoporous carbon nitride and its function as a lipase immobilization support, J. Mater. Chem. 21 (2011) 3890, https://doi.org/10.1039/C0JM03666H.
[22] Y. Wang, N. Zhang, R. Hübner, D. Tan, M. Löffler, S. Facsko, E. Zhang, Y. Ge, Z. Qi, C. Wu, Enzymes Immobilized on Carbon Nitride (C_3N_4) Cooperating with Metal Nanoparticles for Cascade Catalysis, Adv. Mater. Interfaces (2019) 1801664, https://doi.org/10.1002/admi.201801664.

[23] Y. Li, Z. Ruan, M. Zheng, Q. Deng, S. Zhang, C. Zheng, H. Tang, F. Huang, J. Shi, Candida rugosa lipase covalently immobilized on facilely-synthesized carbon nitride nanosheets as a novel biocatalyst, RSC Adv. 8 (2018) 14229, https://doi.org/10.1039/c8ra00536b.
[24] A.A. Mendes, R.C. Giordano, R. de LC Giordano, H.F. de Castro, Immobilization and stabilization of microbial lipases by multipoint covalent attachment on aldehyderesin affinity: application of the biocatalysts in biodiesel synthesis, J. Mol. Catal. B Enzym. 68 (1) (2011) 109–115. https://doi.org/10.1016/j.molcatb.2010.10.002.
[25] P. Yan, D. Li, X. Ma, J. Xue, Y. Zhang, M. Liu, Hydrothermal synthesis of Bi2WO6 with a new tungsten source and enhanced photocatalytic activity of Bi2WO6 hybridized with C3N4, Photochem. Photobiol. Sci. 17 (8) (2018), https://doi.org/10.1039/x0xx00000x.
[26] X. Gao, J. Feng, D. Su, Y. Ma, G. Wang, H. Ma, J. Zhang, In-situ exfoliation of porous carbon nitride nanosheets for enhanced hydrogen evolution, Nano Energy 59 (2019) 598–609, https://doi.org/10.1016/j.nanoen.2019.03.016.
[27] K. Wang, S. Sun, B. Ma, F. Dong, T. Huo, X. Li, Y. Zhao, H. Yu, Y. Huang, Construction and characterization of a nanostructured biocatalyst consisting of immobilized lipase on aminopropyl-functionalized montmorillonite, Appl. Clay Sci. 183 (2019), https://doi.org/10.1016/j.clay.2019.105329 105329.
[28] N. Carrillo, E.A. Ceccarelli, O.A. Roveri Choi, Usefulness of Kinetic Enzyme Parameters in Biotechnological Practice, Sci. Rep. 7 (2017) 17018, https://doi.org/10.1080/02648725.2010.10648157.
[29] S. Kashefi, S.M. Borghei, N.M. Mahmoodi, Covalently immobilized laccase onto graphene oxide nanosheets: Preparation, characterization, and biodegradation of azo dyes in colored wastewater, J. Mol. Liq. 276 (2019) 153–162, https://doi.org/10.1016/j.molliq.2018.11.156.
[30] S.H. Albayati, M. Masomian, S. Nor Hasmah, I.M.S. bin Mohamad Ali, A.L. Thean, F. M. Shariff, N.D. Muhd Noor, R.N.Z. Raja Abd Rahman, Main Structural Targets for Engineering Lipase Substrate Specificity, Catal 10 (2020)747. https://doi:10.3390/catal10070747.
[31] Z. Guan, Q. Li, B. Shen, S. Bao, J. Zhang, B. Tian, Fabrication of Co_3O_4 and Au co-modified BiOBr flower-like microspheres, with high photocatalytic efficiency for sulfadiazine degradation, Sep. Purif. Technol. 234 (2020), https://doi.org/10.1016/j.seppur.2019.116100 116100.
[32] A. Vázquez, D. Hernández-Uresti, S. Obregón, Electrophoretic deposition of CdS coatings and their photocatalytic activities in the degradation of tetracycline antibiotic, Appl. Surf. Sci. 386 (2016) 412–417, https://doi.org/10.1016/j.apsusc.2016.06.034.
[33] C. García-Delgado, E. Eymar, R. Camacho-Arévalo, M. Petruccioli, S. Crognalec, A. D'Annibale, Degradation of tetracyclines and sulfonamides by stevensite- and biochar-immobilized laccase systems and impact on residual antibiotic activity, J. Chem. Technol. Biotechnol. 93 (2018) 3394–3409, https://doi.org/10.1002/jctb.5697.
[34] H. Ding, Y. Wu, B. Zou, Q. Lou, W. Zhang, J. Zhong, L. Lu, G. Dai, Simultaneous removal and degradation characteristics of sulfonamide, tetracycline, and quinolone antibiotics by laccase-mediated oxidation coupled with soil adsorption, J. Hazard. Mater. 307 (2016) 350–358, https://doi.org/10.1016/j.jhazmat.2015.12.062.
[35] S. Jiao, S. Zheng, D. Yin, L. Wang, L. Chen, Aqueous photolysis of tetracycline and toxicity of photolytic products to luminescent bacteria, Chemosphere 73 (3) (2008) 377–382, https://doi.org/10.1016/j.chemosphere.2008.05.042.
[36] F. Hayati, A.A. Isari, B. Anvaripour, M. Fattahi, B. Kakavandi, Ultrasound-assisted photocatalytic degradation of sulfadiazine using MgO@CNT heterojunction composite: Effective factors, pathway and biodegradability studies, Chem. Eng. J. 381 (2020), https://doi.org/10.1016/j.cej.2019.122636 122636.
[37] M.D.G. de Luna, L.K.B. Paragas, R.-A. Doong, Insights into the rapid elimination of antibiotics from aqueous media by tunable C_3N_4 photocatalysts: Effects of dopant amount, co-existing ions and reactive oxygen species, Sci. Total Environ. 669 (2019) 1053–1061, https://doi.org/10.1016/j.scitotenv.2019.03.003.
[38] J. Zdarta, K. Jankowska, K. Bachosz, E. Kijeńska-Gawrońska, A. Zgoła-Grześkowiak, E. Kaczorek, T. Jesionowski, A promising laccase immobilization using electrospun materials for biocatalytic degradation of tetracycline: Effect of process conditions and catalytic pathways, Catal. Today 348 (2020) 127–136, https://doi.org/10.1016/j.cattod.2019.08.042.
[39] X. Yuan, S. Qu, X. Huang, X. Xue, C. Yuan, S. Wang, L. Wei, P. Cai, Design of Core-shelled g-C3N4@ZIF-8 Photocatalyst with Enhanced Tetracycline Adsorption for Boosting Photocatalytic Degradation, Chem. Eng. J. https://doi.org/10.1016/j.cej.2021.129148.
[40] Y. Wu, X. Zhao, S. Huang, Y. Li, X.n Zhang, G. Zeng, L. Niu, Y. Ling, Y. Zhang, Facile construction of 2D g-C3N4 supported nanoflower-like NaBiO3 with direct Z-scheme heterojunctions and insight into its photocatalytic degradation of tetracycline, J. Hazard. Mater., https://doi.org/10.1016/j.jhazmat.2021.125547
[41] M. Li, C. Lai, H. Yi, D. Huang, L. Qin, X. Liu, B. Li, S. Liu, M. Zhang, Y. Fu, L. Li, J. He, Y. Zhang, L. Chen, Multiple charge-carrier transfer channels of Z-scheme bismuth tungstate-based photocatalyst for tetracycline degradation: transformation pathways and mechanism, J. Colloid Interface Sci. 555 (2019) 770–782. https://doi.org/10.1016/j.jcis.2019.08.035
[42] T. Pan, D.D. Chen, W.C. Xu, J.Z. Fang, S.X. Wu, Z. Liu, K. Wu, Z.Q. Fang, Anionic polyacrylamide-assisted construction of thin 2D–2D WO3/g-C3N4 Step-scheme heterojunction for enhanced tetracycline degradation under visible light irradiation, J. Hazard. Mater. 393 (2020), https://doi.org/10.1016/j.jhazmat.2020.122366 122366.
[43] Y. Song, J. Tian, S. Gao, P. Shao, J. Qi, F. Cui, Photodegradation of sulfonamides by g-C_3N_4 under visible light irradiation: Effectiveness, mechanism and pathways, App. Catal. B. 210 (2017) 88–96, https://doi.org/10.1016/j.apcatb.2017.03.059.
[44] H. Zenga, H. Zhanga, L. Deng, Z. Shi, Peroxymonosulfate-assisted photocatalytic degradation of sulfadiazine using self-assembled multi-layered CoAl-LDH/g-C_3N_4 heterostructures: Performance, mechanism and eco-toxicity evaluation, J. Water Process Eng. 33 (2020), https://doi.org/10.1016/j.jwpe.2019.101084 101084.
[45] P. Gholamia, A. Khataee, B. Vahide, A. Karimi, M. Golizadeh, M. Ritala, Sonophotocatalytic degradation of sulfadiazine by integration of microfibrillated carboxymethyl cellulose with Zn-Cu-Mg mixed metal hydroxide/g-C_3N_4 composite, Sep. Purif. Technol. 245 (2020), https://doi.org/10.1016/j.seppur.2020.116866 116866.